Macromolecules

pubs.acs.org/Macromolecules Article

Knots are Generic Stable Phases in Semiflexible Polymers

Suman Majumder,* Martin Marenz, Subhajit Paul, and Wolfhard Janke*

Cite This: *Macromolecules* 2021, 54, 5321−5334 Read Online

ACCESS | Metrics & More | Article Recommendations

ABSTRACT: Semiflexible polymer models are widely used as a paradigm to understand structural phases in biomolecules including folding of proteins. Since stable knots are not so common in real proteins, the existence of stable knots in semiflexible polymers has not been explored much. Here, via extensive replica exchange Monte Carlo simulation, we investigate the same for a bead-stick and a bead-spring homopolymer model that covers the whole range from flexible to stiff. We establish the fact that the presence of stable knots in the phase diagram is dependent on the ratio r_b/r_{min} where r_b is the equilibrium bond length and r_{min} is the distance for the strongest nonbonded contacts. Our results provide evidence for both models that if the ratio r_b/r_{min} is outside a small window around unity, then depending on the bending stiffness, one always encounters stable knotted phases along with the usual frozen and bent-like structures at low temperatures. These findings prompt us to conclude that knots are generic stable phases in semiflexible polymers.

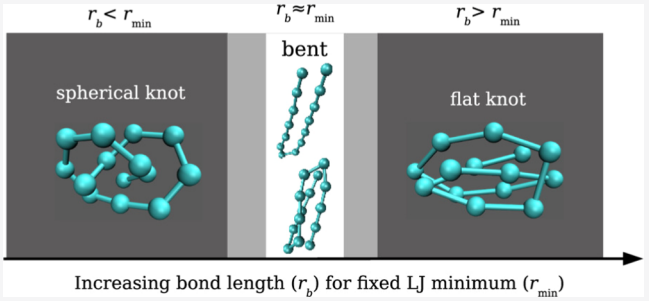

INTRODUCTION

Identification and prediction of macromolecular conformations via computer simulations have developed so much over the years with the current possibility of doing them at atomistic or even at the quantum level. Those detail simulations are always limited by their accessible time scales which often may be too small to provide meaningful insights or it may require enormous effort to arrive at the same. On the other hand, computationally less-expensive coarse-grained approaches (by integrating out certain unimportant degrees of freedom) are more than sufficient to understand the generic behavior of macromolecules.[1] The very simple idea of consideration of self-avoidance and introduction of attraction led to the exploration of theta polymers that are characterized by collapse and freezing transitions.[2] In this regard, even simple lattice models could provide a deep insight.[3−8] The more generic off-lattice models come in two major variants, viz., the bead-stick model and the bead-spring model. They have widely been used to investigate different structural phases of polymers, be it a single one[9−14] or in aggregates[14−17] in bulk, and in some cases, on surfaces[18−22] or under geometrical constraints.[23,24]

While dealing with these models, one should always be aware of the effect of bending stiffness that is used as a parameter to distinguish a flexible polymer from a semiflexible or a stiff one. In this context, a simple worm-like chain model is sufficient to emulate bending-energy-dominated polymers or semiflexible polymers.[25] Such an approach nicely mimics several features of complex biopolymers that include DNA, RNA, and even some proteins. Since the worm-like chain model does not take the self-avoidance or any nonbonded interactions into consideration, it fails to capture the structural transitions associated with a theta polymer. Thus, for a complete understanding, combining the features of theta polymers with the bending stiffness is necessary. From this point of view, using a bead-spring model, Seaton et al.[12] explored different phases (coiled, collapsed, frozen, bent, hairpin, and toroidal conformations) of a semiflexible polymer just by tuning the bending stiffness. Recently, we have shown that similar phases can also be realized if a bead-stick model is used instead.[13] Intriguingly, in addition to those phases there, we have discovered new pseudo-phases characterized by thermodynamically stable knotted structures of the polymer.

Strictly, knots are topological properties of closed strings, and hence, knots found in open polymers are not mathematically defined.[26] Nevertheless, by means of a special strategy for ring closure, the definition can be extended to open polymers as well. Thus, the presence of knots in polymers has fascinated chemists and physicists for long.[27−32] Special interest has evolved around investigating knots in proteins which are best described using semiflexible polymer models. Those studies reveal that only a small fraction of them form knots.[33−36] There have been attempts to understand this fact by arguing that knotted proteins are evolutionarily unfavorable.[37]

Received: November 19, 2020
Revised: April 19, 2021
Published: June 1, 2021

In contrast to proteins, the chances of realizing a knot are higher in flexible polymers either in the swollen or globular phase.[30,32,38,39] The knots identified in most of these studies are formed by chance and cannot be considered to characterize true thermodynamically stable phases. Only recently, in our simulations of a bead-stick semiflexible polymer model where almost the whole range of possible bending stiffnesses was explored, we found stable knots.[13] However, as mentioned earlier in their comprehensive study of the phase diagram of a semiflexible polymer using a bead-spring model, Seaton et al.[12] did not mention any presence of knotted conformations. This poses the important question whether knots are generic phases only in bead-stick polymers. In ref 13, it has been conjectured that the formation of knots is dependent on the ratio of the equilibrium bond length r_b and the distance r_{min} for which the energy due to nonbonded contacts attains its minimum. In this work, we take up this task and study how the ratio r_b/r_{min} influences the presence of stable knots in the phase diagram using both a bead-stick and a bead-spring model. Using the bead-spring model will be particularly helpful in explaining the missing knots in the model used in ref 12. Our results provide evidence that for both the bead-stick and the bead-spring model, knotted structures form a stable phase covering a range of bending stiffnesses if the ratio r_b/r_{min} is away from a small region around unity. This can be explained by analyzing the competition between the nonbonded energy minimization and the bending energy minimization.

The rest of the paper is organized as follows. Next, in the Simulation Details section, we explain the two different models we will be using, the setup of the replica exchange (RE) simulation method, and the data analysis procedure. The details of the bead-spring model employed in ref 12 are relegated to the Appendix. Our main findings are presented in the Results section. Finally, we present a summary and discussion in the Conclusions section.

SIMULATION DETAILS

Models. As already outlined above, we consider two semiflexible polymer models: (i) bead-stick and (ii) bead-spring. In both models, the monomers are considered to be spherical beads with diameter σ, and the nonbonded interaction energy is dependent on the interparticle distance r_{ij} and is given as

$$E_{nb} = \sum_{i=1}^{N-2} \sum_{j=i+2}^{N} [E_{LJ}(\min\{r_{ij}, r_c\}) - E_{LJ}(r_c)] \tag{1}$$

where

$$E_{LJ}(r_{ij}) = 4\varepsilon\left[\left(\frac{\sigma}{r_{ij}}\right)^{12} - \left(\frac{\sigma}{r_{ij}}\right)^{6}\right] \tag{2}$$

is the standard Lennard–Jones (LJ) potential which has a minimum at $r_{min} = 2^{1/6}\sigma$. In eq 1, N is the length of the polymer measured as the total number of beads or monomers. In order to be consistent with our previous study,[13] for the bead-stick model, we set $\sigma = 1.0$ and do not use any cutoff in E_{nb}, whereas for the bead-spring model, we choose $\sigma = 2^{-1/6}$ in order to be consistent with the choice of $r_{min} = 1.0$ in ref 12 and set $r_c = 2.5\sigma$ for faster computation of E_{nb}. For both models, the nonbonded interaction strength ε is set to unity. In bead-stick models, the monomers form a chain where the connectivity between successive monomers is maintained via rigid bonds having fixed length r_b. On the other hand, in a bead-spring model, the bonds between successive monomers are maintained via some kind of springs. Here, we consider the standard finitely extensible nonlinear elastic (FENE) potential[40,41]

$$E_{FENE} = -\frac{K}{2}R^2\sum_{i=1}^{N-1} \ln\left[1 - \left(\frac{r_{ii+1} - r_b}{R}\right)^2\right] \tag{3}$$

where r_b is the equilibrium bond distance for which E_{FENE} is minimum. Unless otherwise mentioned, in all the simulations, we have used $R = 0.3$ and $K = 40$.

In both models, stiffness is introduced via the well-known discretized worm-like chain cosine potential given as

$$E_{bend} = \kappa\sum_{i=1}^{N-2} (1 - \cos\theta_i) \tag{4}$$

where θ_i is the angle between consecutive bonds and κ controls the effective bending stiffness of the polymer. In this work, we aim to perform simulations of the two models using different values of r_b/r_{min}. For that, we fix the value of $r_{min} = 2^{1/6}$ and 1.0, respectively, for the bead-stick and the bead-spring model (by keeping the respective values of σ in all our simulations) and vary only the equilibrium bond length r_b.

Simulation Method. It is known that the phase diagram of coarse-grained semiflexible polymers contains "strong" first-order phase transitions, where "strong" means that the two coexisting phases are separated in phase space by a highly suppressed region.[13,42] On top of that, such systems obey very slow dynamics at low temperatures, even far away from these phase transitions. This demands application of relatively complex Monte Carlo (MC) simulation methods to obtain well-equilibrated results.[13,43] Previously, we have used a parallelized version of the multicanonical algorithm[44−46] along with RE (also known as parallel tempering)[47] and the two-dimensional replica exchange method (2D-RE).[13] Both of them were shown to produce the same results and hence here, we restrict ourselves to use only the 2D-RE algorithm. It is based on many individual Metropolis MC simulations which run in parallel, each at a different parameter pair (T, κ) of temperature T and bending stiffness κ, whose conformations are exchanged every now and then. This substantially improves the quality of the canonical estimates near the phase transitions and also at low temperatures.

For 2D-RE, it is necessary to write down the system Hamiltonian in the following form

$$H = E_0 + \kappa E_1 \tag{5}$$

where E_0 corresponds to the base energy coming from the nonbonded interaction defined in eq 1 and the bonded interaction (if any) in eq 3 and E_1 corresponds to the energy contribution coming from the bending stiffness term $\sum_{i=1}^{N-2}(1 - \cos\theta_i)$ defined in eq 4. While interchanging replicas between two neighboring points μ and ν, in the simulation parameter space (T, κ), the abovementioned splitting of the total energy is used to calculate the exchange probability as

$$p(\mu \leftrightarrow \nu) = \min[1, \exp(\Delta\beta\Delta E_0 + \Delta(\beta\kappa)\Delta E_1)] \tag{6}$$

where $\beta = 1/k_BT$ ($k_B = 1$ being the Boltzmann constant). The two-dimensional parameter space has the advantage that it can

https://doi.org/10.1021/acs.macromol.0c02584
Macromolecules 2021, 54, 5321−5334

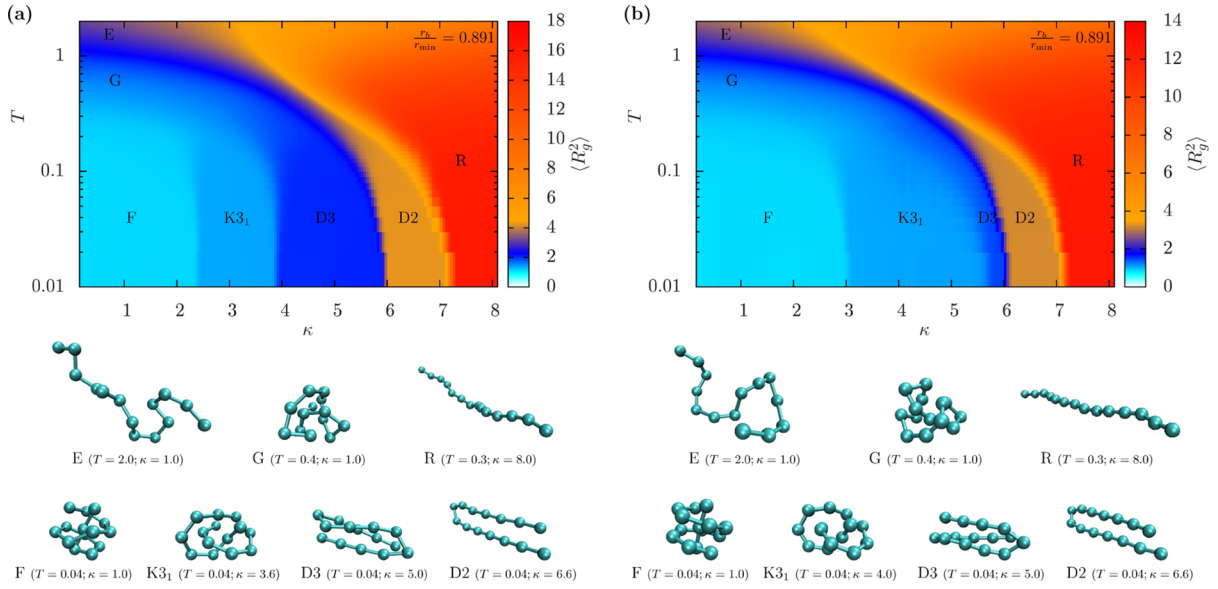

Figure 1. Complete phase diagram for the (a) bead-stick model and (b) bead-spring model with the usual choice of the ratio $r_b/r_{min} = 0.891$ for $N = 14$. The surface plots are drawn with respect to the spatial extension of the polymer chain measured in terms of the squared radius of gyration $\langle R_g^2 \rangle$. The labeled phases stand for the following: E for elongated; R for rod-like; G for globular; F for frozen; KC$_n$ for the knotted phase with the corresponding knot type C_n; and Dn for bent phases with n being the number of segments.

avoid topological barriers which would hinder the flux in a one-dimensional parallel tempering simulation. In one-dimensional parallel tempering simulation, it can happen that there are some temperatures T where almost no state exchange occurs which can be avoided in 2D-RE via exchange along the other direction (κ) in the parameter space (T, κ).

Apart from the 2D-RE algorithm, it is also necessary to adapt different MC update moves to tackle the underlying problem. The set of updates includes the usual crank-shaft, spherical-rotation, and pivot moves for both the bead-stick and bead-spring models.[48] For the bead-spring model, we have also used the single monomer displacement moves. In addition to these standard but simple moves, we have also used the complex double-bridge and bridge-end moves.[49,50] Note that for the bead-stick model, the bridge moves are adjusted accordingly with respect to the fixed bond length.

Analysis. Pursuing the 2D-RE simulations allows us to use the two-dimensional version of the weighted histogram analysis (2D WHAM) method for generating appropriate canonical estimates of quantities of interest.[51,52] Here, one starts by measuring two-dimensional histograms $H_i(E_0, E_1)$ at m different parameter pairs $(T,\kappa)_i$ which gives the energy distribution

$$p_i = \frac{H_i(E_0, E_1)}{N_i} \tag{7}$$

where N_i is the number of measurements performed at each individual parameter space point $(T,\kappa)_i$ to generate $H_i(E_0, E_1)$. Using this, one writes down the density of states as

$$\Omega(E_0, E_1) = \frac{\sum_{k=1}^{m} g_k^{-1} p_k(E_0, E_1)}{\sum_{k=1}^{m} N_k g_k^{-1} Z_{\beta_k,\kappa_k}^{-1} \exp[-\beta_k(E_0 + \kappa E_1)]} \tag{8}$$

where $g_k = 1 + 2\tau_k$ accounts for the integrated autocorrelation time τ_k calculated via binning analysis from the time series generated at each parameter point k. In eq 8, the partition function is given as

$$Z_{\beta_i,\kappa_i} = \sum_{E_0,E_1} \frac{\sum_{k=1}^{m} g_k^{-1} p_k(E_0, E_1)}{\sum_{k=1}^{m} N_k g_k^{-1} Z_{\beta_k,\kappa_k}^{-1} \exp[-\beta_k(E_0 + \kappa E_1)]} \exp[-\beta_i(E_0 + \kappa E_1)] \tag{9}$$

where a priori the values of Z_{β_i,κ_i} are unknown. Assuming appropriate initial values of Z_{β_i,κ_i}, the m self-consistent equations in eq 9 are solved to arrive at precise values of Z_{β_i,κ_i} and thus $\Omega(E_0, E_1)$ via eq 8.[53] Once this is done, the estimate of any observable O at any parameter point (T, κ) can be calculated via

$$\langle O \rangle_{\beta,\kappa} = \frac{\sum_{E_0,E_1} O(E_0, E_1)\Omega(E_0, E_1)\exp[-\beta(E_0 + \kappa E_1)]}{\sum_{E_0,E_1} \Omega(E_0, E_1) \exp[-\beta(E_0 + \kappa E_1)]} \tag{10}$$

In our analyses, we will be dealing with derivatives of certain observables with respect to temperature T calculated as

$$\frac{\mathrm{d}}{\mathrm{d}T}\langle O \rangle = k_B\beta^2(\langle OE \rangle - \langle O \rangle\langle E \rangle) \tag{11}$$

where $E = E_0 + \kappa E_1$ is the total energy. The statistical errors on all the observables are obtained via the Jackknife method.[54] Different observables that we measure during our simulations will be explained subsequently in the Results section.

RESULTS

As already mentioned, we aim to explore the effect of the ratio r_b/r_{min} on the presence of stable knotted phases or in general different phases in both models described above. Thus, subsequently, all the results are organized with respect to the choice of r_b/r_{min}. In the following, we report results for polymers of length $N = 14$ and 28. This choice is motivated by the not too high complexity of the pseudo-phase diagrams and

https://doi.org/10.1021/acs.macromol.0c02584
Macromolecules 2021, 54, 5321−5334

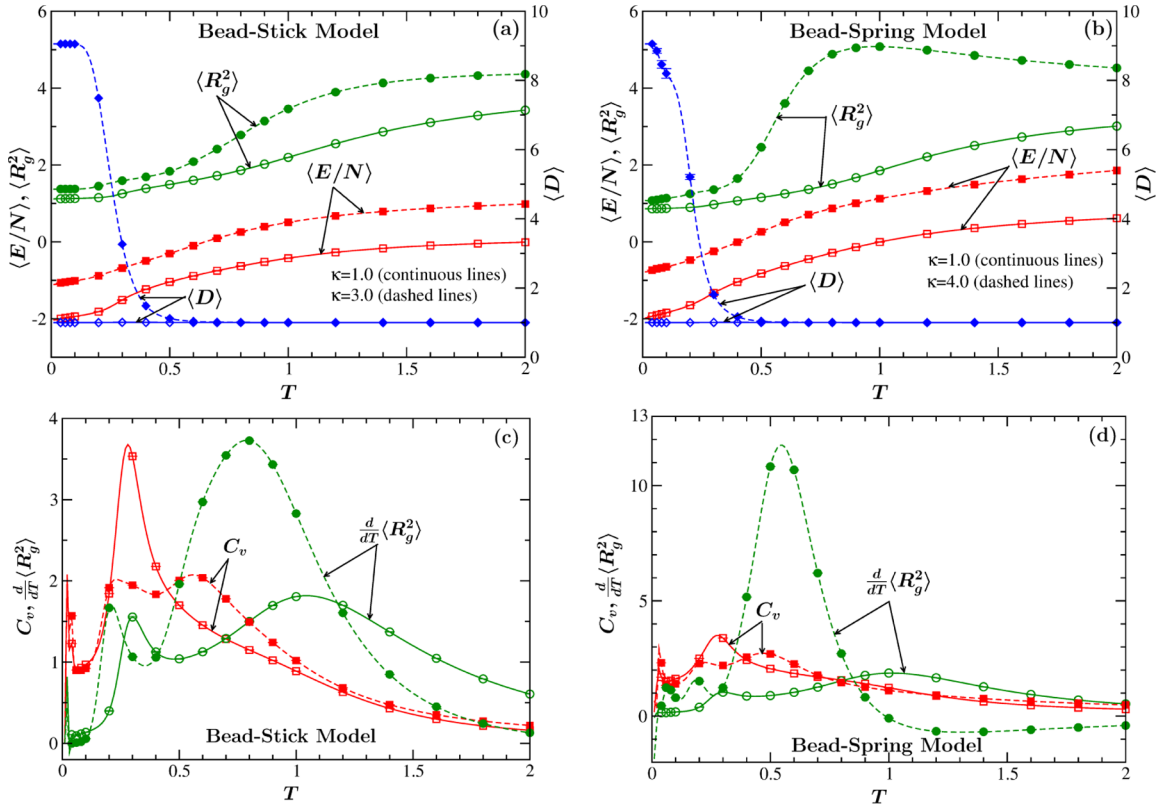

Figure 2. Plots in (a,b) show the validity of the measured quantities, viz., energy density $\langle E/N \rangle$, the squared radius of gyration $\langle R_g^2 \rangle$, and the knot parameter $\langle D \rangle$, to identify the expected transitions between different phases, respectively, for the two models. The quantities are plotted as a function of temperature T with two different choices of the bending stiffness κ as mentioned within (a,b). Plots in (c,d) show the corresponding plots for indirectly measured quantities, viz., specific heat $C_v = d\langle E \rangle/dT$ and the derivative of the squared radius of gyration $d\langle R_g^2 \rangle/dT$, for the two models. All the data presented here are for the choice of $r_b/r_{min} = 0.891$ and $N = 14$.

at the same time will be sufficient to understand the effect of varying r_b/r_{min} on the existence of stable knots.

Phase Behavior for $r_b/r_{min} = 0.891$. We start our investigation with the choice of $r_b/r_{min} = 2^{-1/6} \approx 0.891$, as was used for the bead-stick model in ref 13. Figure 1a,b shows the complete phase diagram in the temperature T and bending stiffness κ plane, for both models with a chain length $N = 14$. The surface plot to differentiate between the different phases is obtained using the estimated squared radius of gyration $\langle R_g^2 \rangle$ calculated as

$$R_g^2 = \frac{1}{2N^2} \sum_{i,j=1}^{N} (\vec{r}_i - \vec{r}_j)^2 \tag{12}$$

where $\vec{r}_i$ is the position vector of the ith monomer. R_g^2 gives a measure of the spatial extension of the polymer. For both models, a rich variety of phases can be observed. Elongated (E) and rod-like (R) conformations are obtained as the two major structures in the noncondensed state, respectively, at low and high κ. In the condensed phases, depending on the bending stiffness and temperature, one observes interesting conformations that range from usual frozen state (F) to bent phases (Dn). Most importantly, like in the bead-stick model (already demonstrated in ref 13), the bead-spring model, too, shows the existence of a knotted phase in the range $\kappa \in [3.2, 5.8]$ which is even wider than the corresponding range $\kappa \in [2.6, 3.8]$ for the bead-stick model.

Before we proceed further with other values of the r_b/r_{min} parameter, it would be worth to limit ourselves to the quantities which are relevant for identifying the knotted phase. For that, in the present case following the custom, we have estimated from our simulation data the energy density $\langle E/N \rangle$ along with $\langle R_g^2 \rangle$. Both these quantities for a fixed κ do not show any signature of pseudo-phase transition (strictly the term phase transition is used in the thermodynamic limit, i.e., in the large N limit), as evident from the corresponding plots shown in Figure 2a,b for both the bead-stick and bead-spring model, respectively. The cases for the higher value of $\kappa = 3.0$ and 4.0 (shown by the dashed lines in the figure), respectively, for the two models correspond to values within the knotted phase. In fact, these parameters also do not provide strong evidence even for the freezing or collapse transition as expected for the lower $\kappa = 1.0$ [shown by the continuous lines in Figure 2a,b] for both models. For this matter, one can also look at the corresponding derivatives using eq 11, that is, the specific heat $C_v = d\langle E \rangle/dT$ and $d\langle R_g^2 \rangle/dT$ which are presented for both the κ values in Figure 2c,d, respectively, for the two models. The derivative $d\langle R_g^2 \rangle/dT$ seems to provide a clear signature for the collapse transition for both models. For the bead-stick model, the collapse transition temperatures for $\kappa = 1.0$ and 3.0 can roughly be read off as 0.85 and 1.1, respectively, which can also be appreciated with regard to the phase diagram presented in Figure 1a. Similarly, in the case of the bead-spring model, the data for $d\langle R_g^2 \rangle/dT$ provide a reasonable signature of the collapse transition temperatures for both the κ values. The specific heat C_v for both models shows peaks at some respective temperatures that may be identified as the collapse transition temperature. However, they are located at values

https://doi.org/10.1021/acs.macromol.0c02584
Macromolecules 2021, 54, 5321−5334

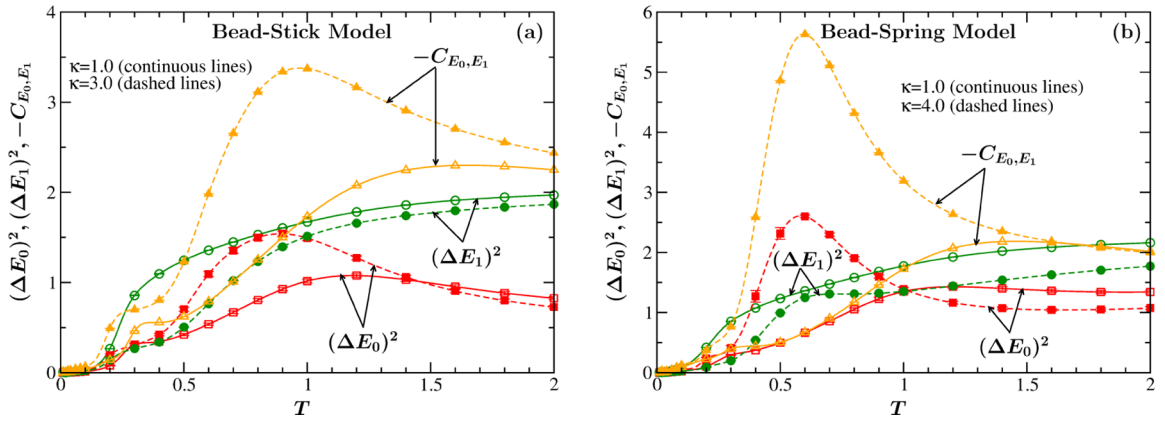

Figure 3. Variance of the base energy $(\Delta E_0)^2$ and the bending energy $(\Delta E_1)^2$ and their cross-correlation C_{E_0,E_1} as a function of temperature with two different choices of κ for the (a) bead-stick and (b) bead-spring model. As in Figure 2, the data are for the choice of $r_b/r_{min} = 0.891$ and $N = 14$.

substantially lower than the corresponding values obtained from $d\langle R_g^2\rangle/dT$. The low-temperature peaks for the $d\langle R_g^2\rangle/dT$ data are prominent for the lower κ values for both models which correspond to the transition to the frozen state F. On the other hand, at low temperature, peaks for the higher κ values for both models are not so pronounced to mark the transition to the stable knotted phase.

In ref 13, using the bead-stick model, it has been pointed out that the transition $K3_1 \leftrightarrow D3$ is first order which is signaled by a bimodal distribution in the two-dimensional space of energies E_0 and E_1. In view of that, we estimate the variances

$$(\Delta E_0)^2 = \langle E_0^2\rangle - \langle E_0\rangle^2 \tag{13}$$

and

$$(\Delta E_1)^2 = \langle E_1^2\rangle - \langle E_1\rangle^2 \tag{14}$$

respectively, for the base energy and the bending energy separately. In Figure 3, the corresponding plots are shown as a function of temperature with the same choices of κ as in Figure 2, for both the models. Clearly, the data do not provide any significant signature of the transition to a knotted phase. As it is intuitive that different phases in a semiflexible polymer result from the interplay of the base energy and the bending energy, we also calculated the cross-correlation between them as

$$C_{E_0,E_1} = \langle E_0E_1\rangle - \langle E_0\rangle\langle E_1\rangle \tag{15}$$

As expected, the results shown in Figure 3 indicate that E_0 and E_1 are anticorrelated. It also provides a signature of the coil-globule transition in both models, especially for the higher κ values. However, C_{E_0,E_1} also fails to capture any signature of the transition to the knotted phase. Thus, we call for an analysis deployed specifically to knots in the polymer.

In a mathematical sense, knots are only defined for closed curves as for the schematics shown in Table 1. An open polymer can satisfy the mathematical definition of a knot only when the termini are closed virtually. For that, we follow ref 55 and first project the polymer conformation onto a 2D plane, as illustrated in Figure 4, for a conformation with a 3_1 knot. One can notice that the mere 2D-projection (say onto the xy plane) yields only one crossing. A direct closure of the termini A and B would also not yield any additional crossing. Therefore, one needs a special closure scheme as demonstrated in the right most panel of Figure 4. There we connect the termini A and B by a straight line, which is then extended in both directions to get two new virtual points C and D located far away from all the monomers. Following that, we create another virtual point E, far away from all the monomers, on the perpendicular bisector of the line AB. The polymer is now closed via straight lines connecting E to C and D, respectively. The resulting closed curve now has two additional crossings making the total number of crossings to be three. The closure is only applied during the measurement of the knot type and does not influence the simulation itself. The details of this closure prescription can be found in refs 13, 32, 55, 56.

Table 1. Expressions for the Alexander Polynomial $\Delta(t)$ and the Corresponding Unique Knot Parameter $D = \Delta_p(-1.1)$ for Some Simple Knots which We Encounter in This Work

Knot type	Schematic	Alexander polynomial $\Delta(t)$	$\Delta_p(-1.1)$
unknotted		1	1.0
3_1		$t+t^{-1}-1$	9.05463
4_1		$-t-t^{-1}+3$	25.09099
5_1		$t^2+t^{-2}-t-t^{-1}+1$	25.45745
8_{19}		$t^3+t^{-3}-t^2-t^{-2}+1$	9.72667

A knot type is denoted as C_n where the integer C counts the minimum number of crossings and the subscript n distinguishes topologically different knots with the same number of crossings.[26] In our study, once the closure is applied, the knot type of the polygonal line describing the polymer is determined in the following way. First, we identify the crossings and then determine the corresponding Alexander

https://doi.org/10.1021/acs.macromol.0c02584
Macromolecules 2021, 54, 5321−5334

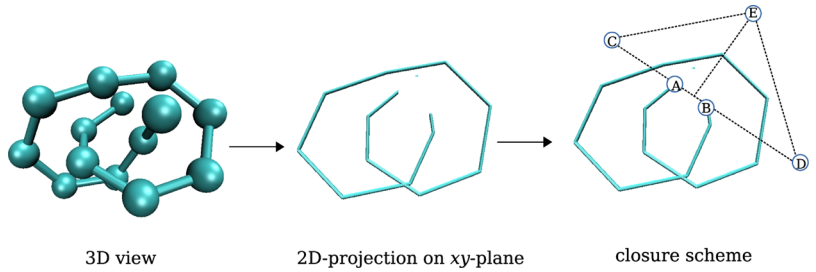

Figure 4. Illustration of the closure scheme to identify the knot type in a polymer. Left panel represents the 3D conformation of a knotted (3_1) polymer. Central panel shows the 2D-projection of the same polymer onto the *xy* plane. The right panel demonstrates the closure applied on the 2D-projection to make the open polymer a closed one.

polynomial invariant.[26] Following ref 32, we avoid unwanted prefactors of the Alexander polynomial $\Delta(t)$ by calculating the variant

$$\Delta_p(t) = |\Delta(t) \times \Delta(1/t)| \tag{16}$$

evaluated at $t = -1.1$. Thus, we define the knot parameter as $D \equiv \Delta_p(-1.1)$. D is also a knot invariant which implies that different polygonal lines with the same knot type correspond to the same D. However, it is not unique as the underlying Alexander polynomial is not unique [e.g., $D(5_1) = D(10_{132})$]. Nevertheless, it is sufficient to distinguish between the simple knots observed in this work. Once the knot parameter D is found for a polymer conformation, one can assign the knot type C_n from a list of possible values of D for simple knots, as presented in Table 1.

The estimated average of the knot parameter $\langle D \rangle$ for the two models is shown in Figure 2a,b, respectively. For the bead-stick and bead-spring polymer with $\kappa = 3.0$ and 4.0, respectively, one can clearly see that at low temperature, $\langle D \rangle$ coincides with the value of $D = 9.05463$ that specifies a trefoil knot (3_1) and at higher T, it drops down to 1 that corresponds to an unknotted polymer. The smooth interpolation across the coexistence region is typical for any phase transition in a finite system (here, the number of monomers $N = 14$). Thus, undoubtedly, the knot parameter is the distinguishing parameter we should be exploring in this work. This can also be appreciated from the plots in Figure 5 showing comparative variation of $\langle E/N \rangle$, $\langle R_g^2 \rangle$, and $\langle D \rangle$ as a function of κ for the temperature fixed to our lowest value of $T = 0.01$. There also, indeed $\langle D \rangle$ provides the most convincing picture for the transition to the knotted phase $K3_1$ for both models. Here, the knot parameter exhibits very sharp and clearly detectable jumps at the phase boundaries to the frozen F and bent D3 phases, respectively, cf. Figure 1. Only a very careful look reveals that this is also reflected by the very small jumps in $\langle R_g^2 \rangle$. Instead of using directly the knot parameter $\langle D \rangle$ in Figures 2 and 5, one could also use the probability of finding a knotted conformation. For the present case, this would provide exactly the same quantitative behavior since there exists only one knot type (3_1) for $N = 14$. In this case, the knot probability x is just related to $\langle D \rangle$ via $x = (\langle D \rangle - 1)/(9.05463 - 1)$. For longer chains, as will be shown later, one observes several neighboring knotted phases where a similar mapping is no longer meaningful since the probability of finding a knot would stay 1 across the phase boundaries. In particular, then, the probability of finding a knot will not be sufficient to recognize the existence of neighboring knotted phases. Thus, we opt for using the knot parameter D for subsequent analyses.

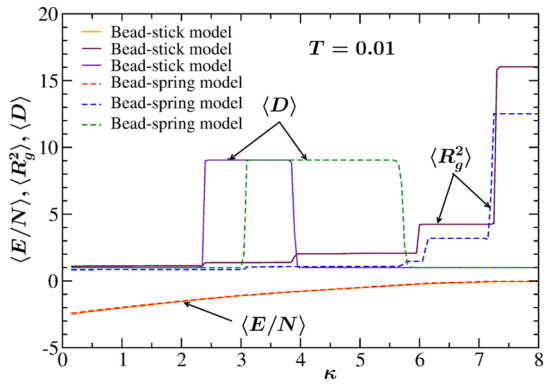

Figure 5. Variation of the energy density $\langle E/N \rangle$, the squared radius of gyration $\langle R_g^2 \rangle$, and the knot parameter $\langle D \rangle$ as a function of the bending stiffness κ for a fixed temperature $T = 0.01$ for both models with the choice of the ratio $r_b/r_{min} = 0.891$ and $N = 14$.

Observation of a knotted structure is not really new; however, in the past, the knotted structures found were by chance and hence were mostly observed in the coiled and globular states. Here, the full phase diagrams shown in Figure 1 indicate that the knotted structures are the stable phases for intermediate values of bending stiffness, especially at low temperatures. This fact raises the question whether there are any entropic contributions to these stable knotted phases. We investigate this in the following empirical approach. We pick up typical conformations from the phases F, $K3_1$, D3, D2, and R at the lowest temperature $T = 0.01$ which can be identified from Figure 1 for both the bead-stick and bead-spring model. Now keeping their morphology intact, we calculate the total energy F_{ps} of each of them just by varying the bending stiffness κ using the Hamiltonian in eq 5. Since this is done at $T = 0.01$ and assuming that the entropic contributions are negligible, it can be considered that one calculates virtually the free energies of the respective conformation while changing κ. Hence, F_{ps} could be termed as the pseudo-free energy of those conformations.

In Figure 6a,b, we present the variation of F_{ps} with κ at $T = 0.01$ for a set of typical conformations, respectively, for the bead-stick and bead-spring model. From the plot, one can easily identify which conformation has the minimal F_{ps} at a particular value of the stiffness κ. For example, when $\kappa = 2.0$ for both models, the frozen conformation (F) has the lowest F_{ps}. Similarly, for $\kappa > 7$, the rod-like (R) conformation has the minimal F_{ps}. This observation is in concurrence with the full phase diagrams presented in Figure 1 for both models. If one starts at $\kappa = 0$ and moves on with increasing κ, at some value of κ, the 3_1 knot takes over the frozen conformation as the

https://doi.org/10.1021/acs.macromol.0c02584
Macromolecules 2021, 54, 5321−5334

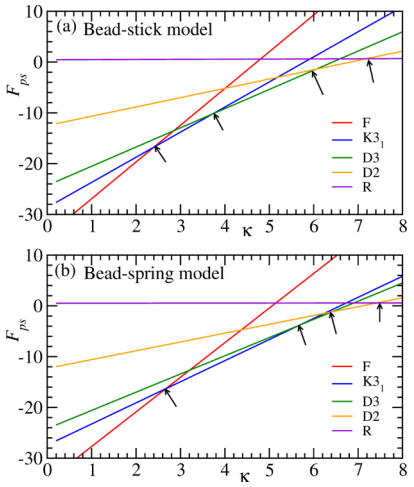

Figure 6. Variation of the calculated pseudo-free energy F_{ps} as a function of the bending stiffness κ at a fixed temperature $T = 0.01$. Results for typical conformations identified from the phase diagrams presented in Figure 1 for the (a) bead-stick model and (b) bead-spring model are presented. The arrows there mark the position where the conformation with the minimum energy switches from one structure to the other.

conformation with minimum F_{ps}. This crossover or switching (marked by the arrows in the plots) to different conformations having the minimum F_{ps} happens four times along the κ axis for both models. Interestingly, these crossover points along κ match quite well with the phase boundaries one observes in the full phase diagrams in Figure 1. This confirms that for all these conformations at low temperature, the entropic contribution is indeed negligible.

The variations of the mean energy in Figure 5 for both models are consistently overlapping with each other and are almost indistinguishable. Thus, the wider range for stable knotted conformations in the bead-spring model should be attributed to the interplay of the base energy E_0 and the bending energy κE_1. To have an idea about this interplay, we show in Figure 7a,c for the bead-stick model, the probability density of E_0 and E_1, respectively, for four different values of κ

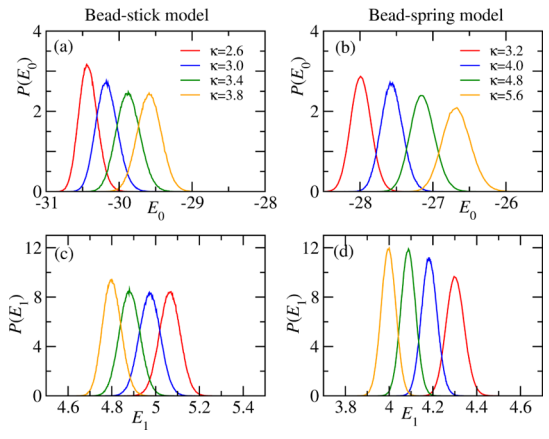

Figure 7. Probability density of the base energy E_0 in the knotted phase for different values of the bending stiffness κ for the (a) bead-stick model and (b) bead-spring model at a temperature $T = 0.01$. Plots in (c,d) show the corresponding probability densities of the energy E_1 ($= E_{bend}/\kappa$) for the two models. All the results are for the ratio $r_b/r_{min} = 0.891$ and $N = 14$.

within the knotted phase at $T = 0.01$. The corresponding plots for the bead-spring model are presented in Figure 7b,d. E_0 for the bead-stick model is the nonbonded energy E_{nb} described in eq 1. For the bead-spring model, E_0 also consists of the bond energy E_{FENE} [as in eq 3], in addition to E_{nb}. E_1 in both models correspond to E_{bend}/κ. Thus, E_1 accounts for the relative orientation of the bonds along the length of the polymer, that is, the factor $\sum_{i=1}^{N-2}(1 - \cos\theta_i)$ in eq 4. From Figure 7a,b, it can be observed that the peak of the distribution of E_0 shifts to the right with the increase in κ for both models. On the other hand, from Figure 7c,d, it is observed that this trend is opposite for E_1, albeit the E_{bend} anyway increases as κ increases. Thus, for both models, it is apparent that a decrease in E_1 is paid off by the increase in E_0. For the bead-spring model, the increase in E_0 per unit change in κ is ≈0.5, which is smaller than the corresponding variation ≈0.83 for the bead-stick model. Similarly, the corresponding decrease in E_1 per unit change in κ within the knotted phase is smaller in the bead-spring model (≈0.125) than in the bead-stick model (≈0.25). This difference comes from the fact that in the bead-spring model since the bond length is not fixed, a variation in the bond lengths may also give rise to an overall better orientation of the bonds such that E_1 is decreased. At very large κ, the overall E_{bend} becomes large and thereby a mild bond orientation is not sufficient to stabilize the structures, and hence, bent structures appear and the knotted phase vanishes. For the bead-stick model, the allowed range of κ is potentially small since the change in bond orientation, that is, decrease in E_1, is only possible due to a pure bond rotation. This provides an intuitive argument why the knotted phase is much wider in the bead-spring model than in the bead-stick model.

Existence of Knots while Varying r_b/r_{min}. From the results obtained in the previous subsection with the ratio $r_b/r_{min} = 0.891$ in both models, we conclude that the formation of a stable knotted phase at low temperatures is guided by the interplay of the base energy E_0 (where E_{LJ} is the sole, respectively, major contribution for the bead-stick or bead-spring model) and the bending energy E_{bend}. Thus, for $r_b/r_{min} = 0.891$, one obtains frozen conformations F where the energy minimization due to the nonbonded contacts can easily overcome the required bending energy penalty (for F, there are a number of bends along the chain that have a bending angle $\theta \approx \pi/2$) for such conformations. As the stiffness κ increases, naturally the number of bends along the chain shall decrease which may give rise to bent conformations such as D3 and D2. However, for this specific choice of $r_b/r_{min} = 0.891$, it is observed that for intermediate values of the stiffness (for both models), knotted conformations are observed. A knotted conformation, such as 3_1, has much less number of severe bends (bending angle $\theta \ll \pi/2$) than a frozen conformation but has sufficient nonbonded contacts courtesy to the crossing or overpassing of the chain onto itself to fulfill the topology of a knot. At even larger values of κ, the nonbonded LJ interaction due to the knot topology is not enough to overcome the bending penalty and thus bent structures such as D3 or D2 become the stable ones. In such a conformation, an energy gain is achieved via the nonbonded LJ contacts of the opposite strands. Now, it is easy to perceive that this strength of the LJ contact is maximum when the distance r_{LJ} between the strands coincides with r_{min} of the model (see Figure 8 for the definition of r_{LJ} in this context). On the other hand, the possible value of this r_{LJ} is correlated with the equilibrium

https://doi.org/10.1021/acs.macromol.0c02584
Macromolecules 2021, 54, 5321−5334

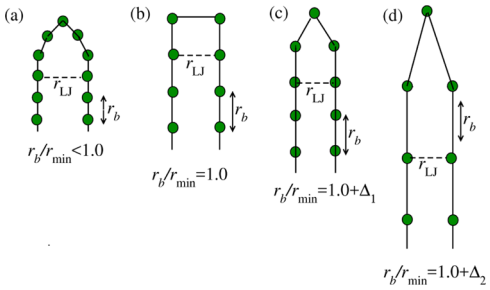

Figure 8. Schematic diagram showing the possible perfectly bent structures one can observe in a semiflexible polymer model with four different choices of the ratio r_b/r_{min} as mentioned. Here, $0 < \Delta_1 < \Delta_2$.

bond length r_b of the conformation (again see Figure 8 to correlate r_b with r_{LJ}). This leads to the inference that the stability of the bent conformations is dependent on the ratio r_b/r_{min}. Since the existence of the knotted phases is dependent on its energetic competition with the bent phases, thus in turn, the very existence of the knotted phases is practically dependent on this ratio r_b/r_{min}.

Before we move on to explore the existence of knots in both models for various choices of the ratio r_b/r_{min}, in Figure 8a–d, we illustrate our speculation about the stability of a bent conformation with D2 as an example. The schematic diagram shows the possible two-dimensional projection of a stable D2 conformation for four different typical choices of r_b/r_{min}. In (a), we have drawn such a schematic for $r_b/r_{min} < 1$. For a short chain of length $N = 14$, in this case, since $r_b < r_{min}$, to have the maximum nonbonded LJ interaction, that is, to have $r_{LJ} = r_{min}$, the bending tip must include several monomers which in turn leave only few monomers to have a real gain in energy due to LJ contact with the opposite strand. Thus, for intermediate values of the bending stiffness, the bent conformations are unstable compared to a trefoil knotted (3_1) conformation (see the typical conformations in Figures 9 and 10 for $r_b/r_{min} = 0.891$). The cases $r_b/r_{min} = 1$ and $r_b/r_{min} = 1 + \Delta_1$ are shown, respectively, in Figure 8b,c. There the minimum number of monomers involved in the bending to form two strands are, respectively, two and three (in general, they must be fewer than in the case of $r_b/r_{min} < 1$). Thus, more monomers can stay on the strands which can now lie easily at a distance $r_{LJ} = r_{min}$, thus minimizing the energies at even intermediate values of the bending stiffness κ. Hence, it seems that for such cases, the bent conformations are always favorable over the simple knotted structure 3_1, possible for relatively short chain length N. However, this is restricted by the value Δ_1. Now let us compare the cases in (b) and (c). In (b), the full turning of the polymer involves two bendings (with $\theta_i = \pi/2$) which accounts for a bending energy 2κ. In this case, for a polymer of length N, the total number of nonbonded contacts will be $(N - 2)/2$ which accounts for an energy gain of $-(N - 2)\varepsilon/2$. For the case in (c), the gain in energy due to nonbonded contacts would be the same as in (b), that is, $-(N - 2)\varepsilon/2$. However, in this case, there are three bends for the full turning of the polymer. Thus, in this case, the relative orientations of these three bonds involved in the turning would decide the total bending energy penalty. Now, if $\sum_i(1 - \cos\theta_i) < 2$, then the conformation in (c) will be even more stable than the corresponding structure in (b). This is dependent on the value of Δ_1. For smaller values of Δ_1, the condition $\sum_i(1 - \cos\theta_i) < 2$ is satisfied and thus the bent structures are even stabler and one would not expect to observe a simple knotted phase in the

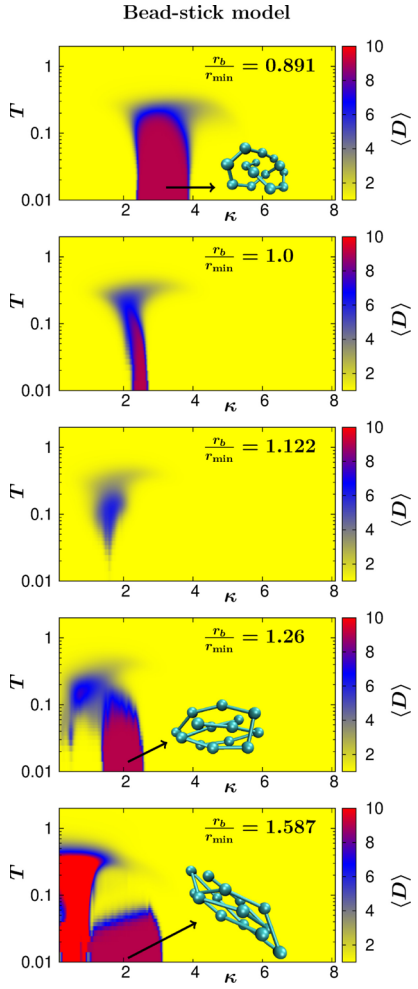

Figure 9. Phase diagram in the (T, κ) plane with the knot parameter $\langle D\rangle$ as the order parameter for a semiflexible polymer with different choices of the ratio r_b/r_{min} using a bead-stick model. The snapshots represent typical polymer conformations in the stable knotted phase having trefoil knots (3_1) for the respective choices of r_b/r_{min}. All the results are for a chain length $N = 14$.

phase diagram. However, if Δ_1 is very large, then $\sum_i(1 - \cos\theta_i) > 2$ and the bent structure in (c) gradually becomes less stable compared to (b) and eventually compared to even a trefoil (3_1) knotted structure (see the typical conformations in Figures 9 and 10 for $r_b/r_{min} = 1.26$ and 1.587). Schematic for such a case, that is, with $r_b/r_{min} = 1 + \Delta_2$ (where $\Delta_2 > \Delta_1$, $r_b \gg r_{min}$), is shown in (d). There one can easily notice that the apex angle θ approaches π, thus making the overall bending energy larger again. In such a situation, thus, we speculate that at low or intermediate values of κ, a simple knotted structure such as 3_1 would be again favorable. From the abovementioned heuristic arguments, we conjecture that for polymers of short length, except for a small window of the ratio $r_b/r_{min} \in [1, 1 + \Delta_1]$, one would expect to observe a knotted phase at low or intermediate values of the bending stiffness.

To check the validity of the abovementioned arguments and how the existence of the knotted phase gets affected by the ratio r_b/r_{min}, we perform simulations with both the bead-stick and bead-spring model for four other choices of $r_b/r_{min} = 1.0$, $2^{1/6}$ (≈1.122), $2^{2/6}$ (≈1.26), and $2^{4/6}$ (≈1.587). Note that this ratio has a lower bound decided by the fact that r_b cannot be less than the diameter σ of the monomer beads. This puts the

https://doi.org/10.1021/acs.macromol.0c02584
Macromolecules 2021, 54, 5321−5334

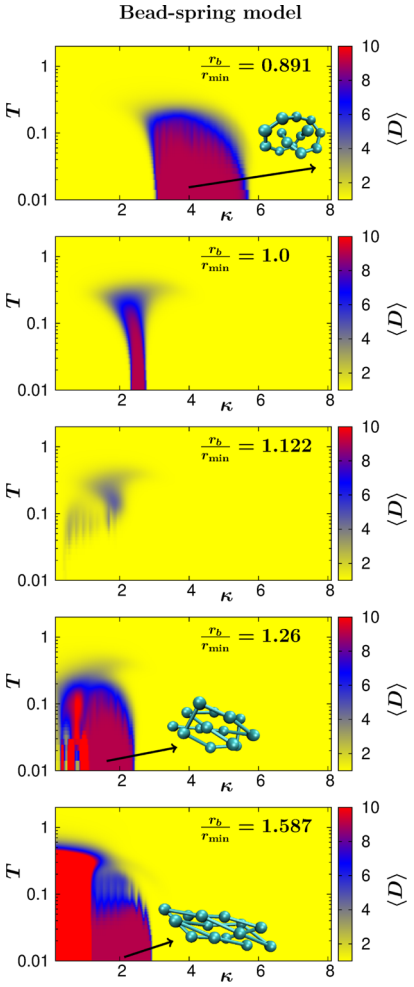

Figure 10. Same as Figure 9 but for the bead-spring model.

lower limit to the ratio $r_b/r_{min} = 2^{-1/6} \approx 0.891$ below which we do not perform any simulations. There is no strict upper bound on r_b/r_{min} but we go up to the value 1.587 beyond which both models show no condensed structure at all for a polymer of length $N = 14$.

Figure 9 shows the results for the bead-stick model which illustrate how the existence of a stable knotted phase gets influenced by the ratio r_b/r_{min}. The phase diagram in the (T, κ) plane is constructed as a surface plot using the knot parameter $\langle D \rangle$. Here, regions with yellow color correspond to unknotted conformations and any other color corresponds to a nonzero probability for knotted conformations. One clearly identifies the knotted phase $K3_1$ (the region represented by the dark red color encoding the value 9.05463) at low temperatures and intermediate bending stiffness κ for all ratios except $r_b/r_{min} = 1.122$. The boundary to the yellow region appears in blue, corresponding to values between 9.05463 and 1, because of the smooth interpolation across the phase boundary for finite systems, already discussed above while looking at the fixed κ and T profiles in Figures 2 and 5. For the case $r_b/r_{min} = 1.0$, the region of the knotted phase is very narrow. This is in concurrence with our speculation that the bent structures are favorable over the knotted ones for the cases presented in Figure 8b,c. We have checked that for $r_b/r_{min} = 1$ and 1.122, alternative structures which appear are D3 and D2. The slightly higher values of $\langle D \rangle$ marked by the blue spot in the phase diagram for $r_b/r_{min} = 1.122$ are due to the presence of few knotted structures mixed with the simple globule. These knots are not stable knots but are formed by chance and are hence of the kind of knotted structures which were reported in the past. Note that since the chain length is relatively short, it is impossible to observe a wide variety of knotted structures. In fact, in all the cases, the observed knots correspond mostly to the trefoil knot 3_1 characterized by $D = 9.05463$ (see Table 1). This can be identified by the red-colored regions in Figure 9. For $r_b/r_{min} = 1.587$, one also notices an orange region at very low κ up to relatively high T. We caution the reader that this does not correspond to the 8_{19} knot with $D = 9.72667$, since a knot with 8 crossings is impossible for a chain length of $N = 14$. An inspection of the time series of D reveals that this region rather corresponds to a mixed phase of 4_1 knots (having $D = 25.09099$) and unknotted conformations. These knots are qualitatively different. They originate in the frozen amorphous (or glass-like) state of the polymer and are highly unstable. Thus, a small perturbation is sufficient to unknot them. The other knot 3_1 is a toroidal knot which reduces the bending energy and is thus stable.

A similar observation can be made from the results of the bead-spring model presented in Figure 10 for the same choices of the ratio r_b/r_{min}. In addition, one can notice that for all the ratios, the width of the knotted phase in the bead-spring model is larger compared to the corresponding width in the bead-stick model. Here, also, the orange region for $r_b/r_{min} = 1.587$ at low κ and covering even relatively higher T corresponds to the mixed phase comprising unknotted and 4_1 knotted structures. Another observation which is in place for both the models is that in contrast to the generic "spherical" knot that one observes for $r_b/r_{min} = 0.891$, for the highest value of $r_b/r_{min} = 1.587$, the knotted conformation looks similar to a bent structure. A careful look in comparison with the bent conformations observed with $r_b/r_{min} = 0.891$ in Figure 1 would reveal that the internal structures are different. In the case of $r_b/r_{min} = 1.587$, the strands penetrate each other giving rise to a "flat" knotted structure, thereby costing bending energy but gaining energy due to additional LJ contacts. In contrast, for $r_b/r_{min} = 0.891$, the strands in the bent structures are almost parallel to each other.

The observed realization of knotted phases in the bead-spring model raises the question why they were not noticed by Seaton et al.[12] with their bead-spring model. The details of this model are discussed in the Appendix. The main difference between their bead-spring model and the model we used is the consideration of the bond energy E_b. In their case, the bonded monomers in addition to an FENE potential also interact via an LJ kind of potential. This makes the effective spring constant that takes care of the elasticity of the bonds much larger, as is shown via the harmonic approximation in the Appendix. Instead of simulating exactly the model of Seaton et al.,[12] we choose to simulate our bead-spring model with a spring constant $K = 297.5$ in eq 3 to be equal to the effective spring constant of the bonds K_{eff} given in eq 26.

The results for the bead-spring model with $K = 297.5$ in the FENE bonds for different choices of the ratio $r_b/r_{min} = 0.891$, 1.0, and 1.26 are presented in Figure 11. In this case also, one can clearly see that for $r_b/r_{min} = 1.0$, the knotted phase region is very narrow in the (T, κ) plane and that it is significantly wider for the cases when $r_b/r_{min} = 0.891$ and 1.26. This again is in accordance with our speculations. Thus, the qualitative behavior is similar to the results presented in Figure 10 where $K = 40$. However, closer inspection reveals that the

https://doi.org/10.1021/acs.macromol.0c02584
Macromolecules 2021, 54, 5321−5334

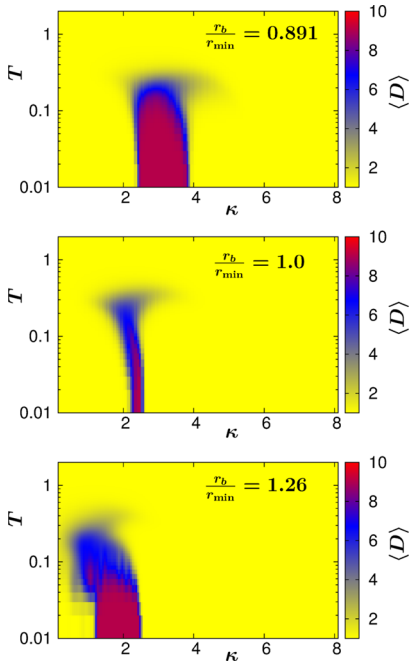

Figure 11. Phase diagram in the (T, κ) plane with the knot parameter $\langle D \rangle$ as the order parameter for a semiflexible polymer with different choices of the ratio r_b/r_{min} using a bead-spring model with the spring constant $K = 297.5$. The results are for a chain length $N = 14$.

ranges of κ over which one sees the knotted phase are [2.4, 3.8] and [1.2, 2.4], respectively, for $r_b/r_{min} = 0.891$ and 1.26, which are smaller than the corresponding ranges for the bead-spring model with $K = 40$. On the contrary, these ranges almost coincide with those we found for the respective values of r_b/r_{min} using the bead-stick model presented in Figure 9. Such a good match with the bead-stick model shows that using such a high value as $K = 297.5$ makes the FENE bonds in the bead-spring model almost as rigid as in the bead-stick case. The realization of a knotted phase in Figure 11 points to the fact that one would have also observed a knotted phase in the model used by Seaton et al. had they used the ratio $r_b/r_{min} = 0.891$ and 1.26. In their study,[12] they used $r_b/r_{min} = 1.0$ for which anyway, we expect the knotted region to be very narrow. Also, the lowest temperature down to which they simulated was $T = 0.03$, for which the chance of detecting the stable knotted phase is really poor. To substantiate our finding, as a step further, we simulated even a longer chain ($N = 28$) using our bead-spring model with $K = 297.5$ and $r_b/r_{min} = 1.0$ (see the Appendix) which in principle is equivalent to the bead-spring model of ref 12. There also, we do not find any stable knotted phase.

Richer Knotted Phase Behavior for Longer Polymers. So far, all the results we have presented are for a polymer of length $N = 14$. There we essentially found the presence of a specific knot type 3_1, the trefoil knot with $D = 9.05463$. This observation of a single knot type is due to the short length which does not allow too many crossings. As expected, if the length increases, the possibility of having many crossings increases which should give rise to a richer variety of knotted structures. It is also quite intuitive that as the length of the polymer increases, the chances of forming knots will be higher. This can be compared with the ease with which one can tie a knot if the given thread is longer. This could explain the formation of the knots which are formed by chance in the coiled or globular phase. Nevertheless, we expect that the likelihood of finding low-temperature stable knotted phases will also increase.

To investigate the existence of knots in longer chains, we now simulate a polymer of length $N = 28$ for both models. This choice of N can be compared with some recent experimental and numerical studies of synthetic polymers adsorbed on a surface in vacuum.[57,58] For each case, we pick two different values of $r_b/r_{min} = 0.891$ and 1.0, for which we speculated to have, respectively, the presence and absence (or a very narrow range) of stable knotted phases. The corresponding phase diagrams for the existence of knots are shown in Figure 12a,b, respectively, for the bead-stick and the bead-spring model. As expected for the ratio $r_b/r_{min} = 0.891$, both models exhibit a stable knotted phase over a wide range of low-to-intermediate bending stiffnesses κ. For the case with $r_b/r_{min} = 1.0$, however, both models show a much smaller window for the knotted phase as observed for the $N = 14$ case.

From the range over which the estimated knot parameter $\langle D \rangle$ varies for both models, it is clear that there exist different knot types indicating a much richer knotted phase behavior

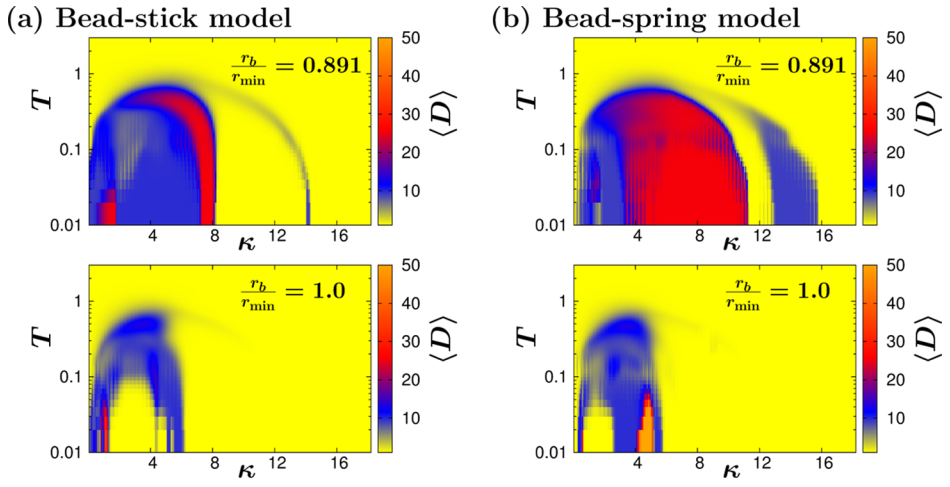

Figure 12. Phase diagram in the (T, κ) plane with the knot parameter $\langle D \rangle$ as the order parameter for a semiflexible polymer of length $N = 28$ using the (a) bead-stick model and (b) bead-spring model. For both models, results for two choices of the ratio $r_b/r_{min} = 0.891$ and 1.0 are presented.

https://doi.org/10.1021/acs.macromol.0c02584
Macromolecules 2021, 54, 5321−5334

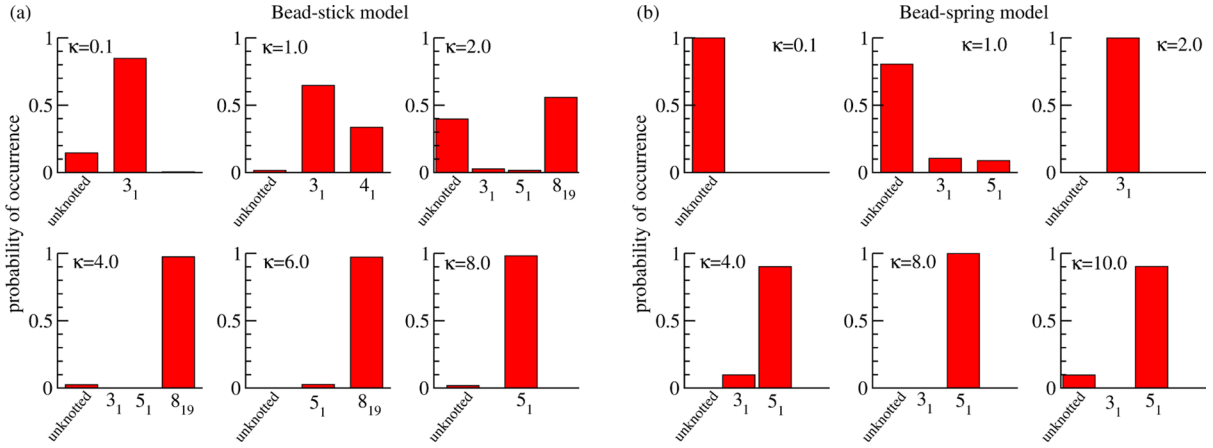

Figure 13. Probabilities of occurrence of different knot types at $T = 0.01$ and at different bending stiffnesses κ for the two models. The results are for a polymer of length $N = 28$ with the ratio $r_b/r_{min} = 0.891$.

compared to the $N = 14$ case. Again, as for $N = 14$, also in the $N = 28$ phase diagrams, the yellow color corresponds to regions with unknotted conformations (knot probability $x = 0$), but here, the non-yellow-colored region corresponds to different knotted phases (knot probability $x = 1$), cf. Figure 1b of ref 13. Here, the color coding is more difficult to interpret than for $N = 14$, but it does contain useful information which would be lost by only displaying the knot probability. The central blue region in Figure 12a for $r_b/r_{min} = 0.891$ shows the 8_{19} knot with $D = 9.72667$ (exceptionally close to the value for the 3_1 knot), the red region to the right encodes the 5_1 knot (with $D = 25.45745$), and the small red region to the left at very low temperatures signals predominantly the 4_1 knot (with $D = 25.09099$). The thin blue band surrounding the red region to the right (and top) is again caused by the interpolation effect (from 25.45745 to 1) across the phase transition to the bent D3 phase. To demonstrate this more clearly, we have calculated the probability of occurrence of specific knot types within the knotted region for the case of $r_b/r_{min} = 0.891$. By examining the knotted structures for both models, we observed that the maximum number of crossings was 8. Thus, at first, we made a list of D values of all the 35 possible knots which have 8 or less crossings. Using this list (for a few selected examples, see Table 1), we now measure the probability of occurrence of specific knot types from our time series data of the knot parameter D. These probabilities for a fixed temperature $T = 0.01$ and for six different κ within the knotted phases of the two models are plotted in Figure 13a,b, respectively. In the bead-stick model with $\kappa = 0.1$ (in the almost flexible limit), one sees the presence of only 3_1 knots along with the unknotted conformations. These are simple knots occurring by chance in the frozen state. For $\kappa = 1.0$, the complexity of the observed knots increases with significant probabilities of finding 3_1 and 4_1 knots. It further increases for $\kappa = 2.0$ where one sees that a major fraction of the conformations are 8_{19} knots. The 8_{19} knot becomes the dominant one for both $\kappa = 4.0$ and 6.0, before the 5_1 knot takes over for $\kappa = 8.0$. A careful view on the colored regions in Figure 12a is in accordance with these facts.

The corresponding plots for the bead-spring model in Figure 13b also show a somewhat similar picture. Noticeable again is the fact that the unknotted phase vanishes at a much smaller $\kappa = 2.0$ compared to the bead-stick model and continues to remain so until $\kappa = 10.0$ indicating a much wider range of stable knotted phases, a fact also encountered for the $N = 14$ polymer. The other noticeable feature is that for the bead-spring model, the stable knotted structure is 5_1 which has less crossings than the corresponding 8_{19} knot for the bead-stick model. This again could be attributed to the presence of E_{FENE} in the nonbonded energy. The presence of the FENE bonds allows the polymers to orient its bonds appropriately and thereby lowering the energy. However, for bead-stick polymers, this is not possible. Instead, they achieve it by additional crossings which give rise to more knotted structures such as 8_{19}.

CONCLUSIONS

We have presented results on the existence of stable knotted phases in semiflexible polymers via extensive RE MC simulations of a bead-stick and bead-spring homopolymer model covering the full range of the bending stiffness κ via which one can tune the polymer from a completely flexible to a stiff one. We speculate that the existence of a knotted phase is dependent on the choice of the ratio r_b/r_{min} between the equilibrium bond length r_b and the distance r_{min} for the maximum nonbonded contact. Via simple qualitative arguments based on the interplay of the energy gain due to nonbonded contacts and the bending energy penalty, it can be understood that for cases where $r_b/r_{min} \neq 1$, the knotted structures are more favorable than the alternative bent structures. This is strongly supported by our simulation results for different choices of r_b/r_{min} for both models.

When the results of the two models are compared, the knotted phase in the bead-spring model is much wider than the corresponding range in the bead-stick model. In this regard, our results for the bead-spring model can be compared with the results of Seaton et al.[12] where they do not mention any existence of knotted structures. This could be due to the use of $r_b/r_{min} = 1.0$ coupled with the fact they did not perform their simulation at low enough temperature compared to ours. Similarly, in a study of a semiflexible polymer adsorbed on a flat surface, no knots were found.[20] This could also be attributed to the fact that there also, $r_b/r_{min} = 1.0$ and the lowest simulation temperature ($T = 0.1$) was much higher than the one where we found the knotted phase in this work. Thus, it would be worth revisiting this issue on the existence of stable knotted structures in polymers adsorbed on surfaces by tuning r_b/r_{min} in the model used. This we take as future endeavor.

https://doi.org/10.1021/acs.macromol.0c02584
Macromolecules 2021, 54, 5321−5334

In conclusion, our results point out that knots are generic phases for semiflexible homopolymers except for a very narrow range of choice of the ratio r_b/r_{min} close to unity. This is in contrast with the corresponding results on the existence of knots in proteins which are typically modeled as semiflexible heteropolymers. A closer look into heteropolymers reveals that this can be plausible due to the following fact. Homopolymers can have substantial energy gain via nonbonded contacts happening due to several crossings or under passing present in a knotted structure. However, for a heteropolymer, such an energy gain is not guaranteed due to the presence of specific hydrophobic and polar sequences. From this point of view, it would also be worth exploring the sequence-dependent formation of knotted structures in a semiflexible heteropolymer which in turn will throw some light on the existence of knots in proteins.

APPENDIX

Harmonic Approximation of the Potentials Used in ref 12

The semiflexible polymer model used by Seaton et al.[11,12] is a bead-spring model where the nonbonded interaction is given by an LJ potential and the bending energy penalty was constructed in the same fashion as we did. The main difference is the bond energy. Following that, we describe the form of potentials they used and subsequently do the harmonic approximation of their bond energy. The nonbonded potential among the monomers is given by

$$E_{nb}(r) = \begin{cases} E_{LJ}(r) - E_{LJ}(r_c) & r < r_c \\ 0 & \text{otherwise} \end{cases} \tag{17}$$

where

$$E_{LJ}(r) = \varepsilon\left[\left(\frac{\sigma}{r}\right)^{12} - 2\left(\frac{\sigma}{r}\right)^{6}\right] \tag{18}$$

and $r_c = 3\sigma$.[11] Here, they choose $\sigma = 1$ and $\varepsilon = 1$ such that $r_{min} = 1$ with $E_{LJ}(r_{min}) = -\varepsilon = -1$ and $E_{LJ}(r)$ in eq 17 agrees exactly with our form for $E_{LJ}(r)$ in eq 2 with $\sigma = 2^{-1/6}$, albeit the cutoff distance $r_c = 3$ is different from our $r_c = 2.5\sigma \approx 2.23$.

The bonded interaction between two monomers consists of a combination of the LJ potential described above and an FENE potential

$$E_b(r) = \begin{cases} E_{LJ}(r) + E_{FENE}(r) & 0 < r \le R_0 \\ 0 & \text{otherwise} \end{cases} \tag{19}$$

The LJ potential in eq 19 has the same form as in eq 17 but the values of the parameters are different which will be discussed below. Here, the FENE potential has the form[59]

$$E_{FENE}(r) = -\frac{K}{2}{R_0}^2 \ln\left[1 - \left(\frac{r}{R_0}\right)^2\right] \tag{20}$$

where R_0 is the finite extensibility and K is the stiffness constant. In dimensionless units, the values were taken as $R_0 = 1.2$ and $K = 2$ by Seaton et al.. Note that their choice of E_{FENE} is different from E_{FENE} we have chosen for our simulations, as given in eq 3.

They determined the parameters of E_{LJ} in such a way that E_b is minimum at bond length $r = r_b = 1$. Thus, setting the first derivative of this bonded potential $(dE_b/dr) = 0$ at $r = r_b$ leads to the equation

$$\frac{12\varepsilon}{r_b}\left[\left(\frac{\sigma}{r_b}\right)^{12} - \left(\frac{\sigma}{r_b}\right)^{6}\right] = \frac{Kr_b}{1 - (r_b/R_0)^2} \tag{21}$$

whose solution with $r_b = 1$ gives us the dependence of σ on ε as (using $R_0 = 1.2$ and $K = 2$),

$$\sigma^6 = \frac{1}{2}\left(1 + \sqrt{1 + \frac{24}{11\varepsilon}}\right) \tag{22}$$

from which by setting $\varepsilon = 2$, one gets $\sigma \approx 1.03412$.[60]

In order to obtain the effective spring constant for the bonded potential, we need to do a Taylor series expansion of $E_b(r)$ around its minimum (r_b) and keep the terms up to the second-order derivative. The expansion gives

$$E_b(r) = E_b(r_b) + (r - r_b)\left.\frac{dE_b}{dr}\right|_{r=r_b} + \frac{(r - r_b)^2}{2}\left.\frac{d^2E_b}{dr^2}\right|_{r=r_b} + \ldots \tag{23}$$

Keeping up to the harmonic approximation (i.e., up to the second derivative) and shifting $E_b(r)$ by $E_b(r_b)$, we get

$$E_b(r) = \frac{K_{eff}}{2}(r - r_b)^2 \tag{24}$$

where

$$K_{eff} = \left.\frac{d^2E_{LJ}}{dr^2}\right|_{r=r_b} + \left.\frac{d^2E_{FENE}}{dr^2}\right|_{r=r_b} \tag{25}$$

Now using the second-order derivatives of both the terms for the bonded potential, we get K_{eff} (for $r_b = 1$) as

$$K_{eff} = 12\varepsilon[13\sigma^{12} - 7\sigma^6] + \frac{K{R_0}^2}{({R_0}^2 - 1)^2}({R_0}^2 + 1) \tag{26}$$

Inserting the values of the parameters ($\varepsilon = 2$, $\sigma = 1.03412$, $R_0 = 1.2$, and $K = 2$) in the abovementioned equation gives the effective value of the spring constant as $K_{eff} \approx 297.5$. As can be seen in Figure 14, for small variations of the bond length, the agreement is excellent.

Using $K = K_{eff}$ in our bead-spring model with $r_b/r_{min} = 1.0$, we now perform RE simulations. The results are summarized in Figure 15 for a polymer with a choice of $N = 28$, consistent with the largest choice we made in the main text. Nevertheless,

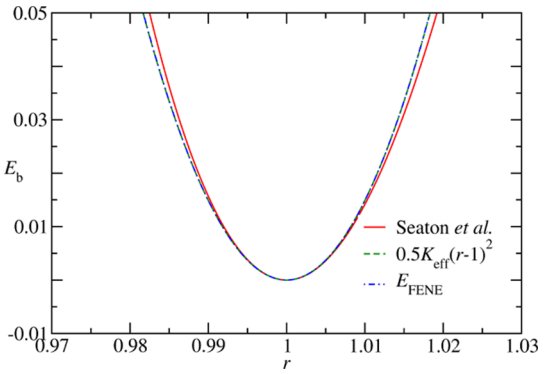

Figure 14. Comparison of the bond potential employed by Seaton et al.,[11,12] a simple harmonic potential with spring constant $K_{eff} = 297.5$ and the FENE potential used by us as in eq 3 with $K = K_{eff}$.

https://doi.org/10.1021/acs.macromol.0c02584
Macromolecules 2021, 54, 5321−5334

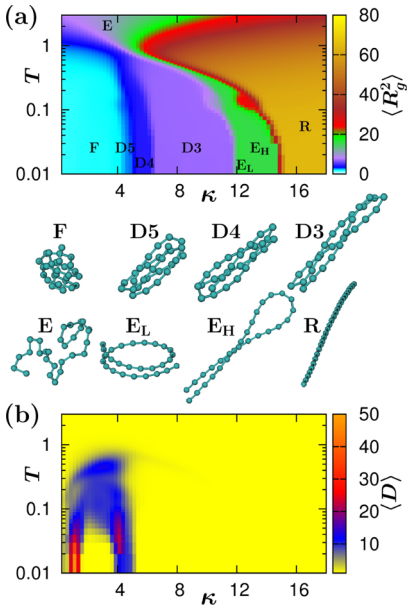

Figure 15. (a) Complete phase diagram for a semiflexible polymer of length $N = 28$ using the bead-spring model with $r_b/r_{min} = 1.0$ and $K = K_{eff} = 297.5$. The surface plot is generated using the estimated squared radius of gyration $\langle R_g^2 \rangle$. The labeled phases stand for the following: E for elongated; R for rodlike; F for frozen; Dn for bent phases with n being the number of segments; E_L for elongated loop; and E_H for hairpin. (b) Corresponding phase diagram using the knot parameter $\langle D \rangle$ as the order parameter.

$N = 28$ is almost as long as in ref 12 where $N = 30$ was chosen. The phase diagram in Figure 15a shows that we also observe the same variety of conformations as was obtained in ref 12 that includes frozen (F), extended coil (E), bent structures (D5, D4, and D3), elongated loop (E_L), hairpin (E_H), and rodlike (R) structures. On the other hand, the phase diagram with the estimated knot parameter $\langle D \rangle$ as the order parameter in Figure 15b shows no stable knotted phase. The blue region in there is only an indication of mixed phases that constitute unknotted frozen structures and knotted structures which we confirmed from the corresponding time series of D.

AUTHOR INFORMATION

Corresponding Authors

Suman Majumder − *Institut für Theoretische Physik, Universität Leipzig, 04081 Leipzig, Germany;* orcid.org/0000-0003-3898-7261; Email: suman.majumder@itp.uni-leipzig.de

Wolfhard Janke − *Institut für Theoretische Physik, Universität Leipzig, 04081 Leipzig, Germany;* orcid.org/0000-0002-5165-9097; Email: wolfhard.janke@itp.uni-leipzig.de

Authors

Martin Marenz − *Institut für Theoretische Physik, Universität Leipzig, 04081 Leipzig, Germany*

Subhajit Paul − *Institut für Theoretische Physik, Universität Leipzig, 04081 Leipzig, Germany*

Complete contact information is available at: https://pubs.acs.org/10.1021/acs.macromol.0c02584

Notes

The authors declare no competing financial interest.

ACKNOWLEDGMENTS

We thank Stefan Schnabel for useful discussion. This project was funded by the Deutsche Forschungsgemeinschaft (DFG, German Research Foundation) under grant nos. JA 483/33-1 and 189 853 844−SFB/TRR 102 (project B04) and the Deutsch-Französische Hochschule (DFH-UFA) through the Doctoral College "$\mathbb{L}^4$" under grant no. CDFA-02-07. It was further supported by the EU COST programme "EUTOPIA" under grant no. CA17139.

REFERENCES

(1) Müller-Plathe, F. Coarse-graining in polymer simulation: From the atomistic to the mesoscopic scale and back. *ChemPhysChem* **2002**, *3*, 754−769.

(2) Lifshitz, I. M.; Grosberg, A. Y.; Khokhlov, A. R. Some problems of the statistical physics of polymer chains with volume interaction. *Rev. Mod. Phys.* **1978**, *50*, 683−713.

(3) Carmesin, I.; Kremer, K. The bond fluctuation method: A new effective algorithm for the dynamics of polymers in all spatial dimensions. *Macromolecules* **1988**, *21*, 2819−2823.

(4) Grassberger, P.; Hegger, R. Simulations of three-dimensional θ polymers. *J. Chem. Phys.* **1995**, *102*, 6881−6899.

(5) Bastolla, U.; Grassberger, P. Phase transitions of single semistiff polymer chains. *J. Stat. Phys.* **1997**, *89*, 1061−1078.

(6) Rampf, F.; Paul, W.; Binder, K. On the first-order collapse transition of a three-dimensional, flexible homopolymer chain model. *Europhys. Lett.* **2005**, *70*, 628−634.

(7) Vogel, T.; Bachmann, M.; Janke, W. Freezing and collapse of flexible polymers on regular lattices in three dimensions. *Phys. Rev. E: Stat., Nonlinear, Soft Matter Phys.* **2007**, *76*, 061803.

(8) Farris, A. C. K.; Shi, G.; Wüst, T.; Landau, D. P. The role of chain-stiffness in lattice protein models: A replica-exchange Wang-Landau study. *J. Chem. Phys.* **2018**, *149*, 125101.

(9) Schnabel, S.; Bachmann, M.; Janke, W. Elastic Lennard-Jones polymers meet clusters: Differences and similarities. *J. Chem. Phys.* **2009**, *131*, 124904.

(10) Schnabel, S.; Vogel, T.; Bachmann, M.; Janke, W. Surface effects in the crystallization process of elastic flexible polymers. *Chem. Phys. Lett.* **2009**, *476*, 201−204.

(11) Seaton, D. T.; Wüst, T.; Landau, D. P. Collapse transitions in a flexible homopolymer chain: Application of the Wang-Landau algorithm. *Phys. Rev. E: Stat., Nonlinear, Soft Matter Phys.* **2010**, *81*, 011802.

(12) Seaton, D. T.; Schnabel, S.; Landau, D.; Bachmann, M. From flexible to stiff: Systematic analysis of structural phases for single semiflexible polymers. *Phys. Rev. Lett.* **2013**, *110*, 028103.

(13) Marenz, M.; Janke, W. Knots as a topological order parameter for semiflexible polymers. *Phys. Rev. Lett.* **2016**, *116*, 128301.

(14) Zierenberg, J.; Marenz, M.; Janke, W. Dilute semiflexible polymers with attraction: Collapse, folding and aggregation. *Polymers* **2016**, *8*, 333.

(15) Zierenberg, J.; Janke, W. From amorphous aggregates to polymer bundles: The role of stiffness on structural phases in polymer aggregation. *Europhys. Lett.* **2015**, *109*, 28002.

(16) Ranganathan, S.; Maji, S. K.; Padinhateeri, R. Defining a physical basis for diversity in protein self-assemblies using a minimal model. *J. Am. Chem. Soc.* **2016**, *138*, 13911−13922.

(17) Midya, J.; Egorov, S.; Binder, K.; Nikoubashman, A. Phase behavior of flexible and semiflexible polymers in solvents of varying quality. *J. Chem. Phys.* **2019**, *151*, 034902.

(18) Sintes, T.; Sumithra, K.; Straube, E. Adsorption of semiflexible polymers on flat, homogeneous surfaces. *Macromolecules* **2001**, *34*, 1352−1357.

(19) Möddel, M.; Janke, W.; Bachmann, M. Adsorption and pattern recognition of polymers at complex surfaces with attractive stripelike motifs. *Phys. Rev. Lett.* **2014**, *112*, 148303.

(20) Austin, K. S.; Zierenberg, J.; Janke, W. Interplay of Adsorption and Semiflexibility: Structural Behavior of Grafted Polymers under Poor Solvent Conditions. *Macromolecules* **2017**, *50*, 4054−4063.
(21) Oberthür, N.; Gross, J.; Janke, W. Two-dimensional Monte Carlo simulations of coarse-grained poly(3-hexylthiophene) (P3HT) adsorbed on striped substrates. *J. Chem. Phys.* **2018**, *149*, 144903.
(22) Milchev, A.; Binder, K. Linear Dimensions of Adsorbed Semiflexible Polymers: What can be learned about their persistence length? *Phys. Rev. Lett.* **2019**, *123*, 128003.
(23) Zierenberg, J.; Mueller, M.; Schierz, P.; Marenz, M.; Janke, W. Aggregation of theta-polymers in spherical confinement. *J. Chem. Phys.* **2014**, *141*, 114908.
(24) Milchev, A.; Egorov, S. A.; Vega, D. A.; Binder, K.; Nikoubashman, A. Densely packed semiflexible macromolecules in a rigid spherical capsule. *Macromolecules* **2018**, *51*, 2002−2016.
(25) Kratky, O.; Porod, G. Röntgenuntersuchung gelöster Fadenmoleküle. *Recl. Trav. Chim. Pays-Bas* **1949**, *68*, 1106−1122.
(26) Kauffman, L. H. *Knots and Physics*, 4th ed.; World Scientific: Singapore, 2013.
(27) Frisch, H. L.; Wasserman, E. Chemical topology[1]. *J. Am. Chem. Soc.* **1961**, *83*, 3789−3795.
(28) Frank-Kamenetskii, M. D.; Lukashin, A. V.; Vologodskii, A. V. Statistical mechanics and topology of polymer chains. *Nature* **1975**, *258*, 398−402.
(29) Liu, L. F.; Depew, R. E.; Wang, J. C. Knotted single-stranded DNA rings: A novel topological isomer of circular single-stranded DNA formed by treatment with Escherichia coli ω protein. *J. Mol. Biol.* **1976**, *106*, 439−452.
(30) Koniaris, K.; Muthukumar, M. Knottedness in ring polymers. *Phys. Rev. Lett.* **1991**, *66*, 2211−2214.
(31) Taylor, W. R.; Lin, K. Protein knots: A tangled problem. *Nature* **2003**, *421*, 25.
(32) Virnau, P.; Kantor, Y.; Kardar, M. Knots in globule and coil phases of a model polyethylene. *J. Am. Chem. Soc.* **2005**, *127*, 15102−15106.
(33) Taylor, W. R. A deeply knotted protein structure and how it might fold. *Nature* **2000**, *406*, 916−919.
(34) Lua, R. C.; Grosberg, A. Y. Statistics of knots, geometry of conformations, and evolution of proteins. *PLoS Comput. Biol.* **2006**, *2*, No. e45.
(35) Virnau, P.; Mirny, L. A.; Kardar, M. Intricate knots in proteins: Function and evolution. *PLoS Comput. Biol.* **2006**, *2*, No. e122.
(36) Jamroz, M.; Niemyska, W.; Rawdon, E. J.; Stasiak, A.; Millett, K. C.; Sułkowski, P.; Sulkowska, J. I. KnotProt: A database of proteins with knots and slipknots. *Nucl. Acids Res.* **2014**, *43*, D306−D314.
(37) Wüst, T.; Reith, D.; Virnau, P. Sequence determines degree of knottedness in a coarse-grained protein model. *Phys. Rev. Lett.* **2015**, *114*, 028102.
(38) Deguchi, T.; Tsurusaki, K. Universality of random knotting. *Phys. Rev. E: Stat., Nonlinear, Soft Matter Phys.* **1997**, *55*, 6245−6248.
(39) Lua, R.; Borovinskiy, A. L.; Grosberg, A. Y. Fractal and statistical properties of large compact polymers: A computational study. *Polymer* **2004**, *45*, 717−731.
(40) Milchev, A.; Paul, W.; Binder, K. Off-lattice Monte Carlo simulation of dilute and concentrated polymer solutions under theta conditions. *J. Chem. Phys.* **1993**, *99*, 4786−4798.
(41) Milchev, A.; Bhattacharya, A.; Binder, K. Formation of block copolymer micelles in solution: A Monte Carlo study of chain length dependence. *Macromolecules* **2001**, *34*, 1881−1893.
(42) Noguchi, H.; Yoshikawa, K. First-order phase transition in a stiff polymer chain. *Chem. Phys. Lett.* **1997**, *278*, 184−188.
(43) Janke, W. Generalized ensemble computer simulations of macromolecules. In *Order, Disorder and Criticality: Advanced Problems of Phase Transition Theory*; Holovatch, Y., Ed.; World Scientific: Singapore, 2018; Vol. 5; pp 173−225.
(44) Berg, B. A.; Neuhaus, T. Multicanonical algorithms for first order phase transitions. *Phys. Lett. B* **1991**, *267*, 249−253.
(45) Zierenberg, J.; Marenz, M.; Janke, W. Scaling properties of a parallel implementation of the multicanonical algorithm. *Comput. Phys. Commun.* **2013**, *184*, 1155−1160.
(46) Janke, W.; Paul, W. Thermodynamics and structure of macromolecules from flat-histogram Monte Carlo simulations. *Soft Matter* **2016**, *12*, 642−657.
(47) Hukushima, K.; Nemoto, K. Exchange Monte Carlo method and application to spin glass simulations. *J. Phys. Soc. Jpn.* **1996**, *65*, 1604−1608.
(48) Austin, K. S.; Marenz, M.; Janke, W. Efficiencies of joint non-local update moves in Monte Carlo simulations of coarse-grained polymers. *Comput. Phys. Commun.* **2018**, *224*, 222−229.
(49) Pant, P. V. K.; Theodorou, D. N. Variable connectivity method for the atomistic Monte Carlo simulation of polydisperse polymer melts. *Macromolecules* **1995**, *28*, 7224−7234.
(50) Karayiannis, N. C.; Mavrantzas, V. G.; Theodorou, D. N. A novel Monte Carlo scheme for the rapid equilibration of atomistic model polymer systems of precisely defined molecular architecture. *Phys. Rev. Lett.* **2002**, *88*, 105503.
(51) Ferrenberg, A. M.; Swendsen, R. H. New Monte Carlo technique for studying phase transitions. *Phys. Rev. Lett.* **1988**, *61*, 2635−2638.
(52) Kumar, S.; Rosenberg, J. M.; Bouzida, D.; Swendsen, R. H.; Kollman, P. A. The weighted histogram analysis method for free-energy calculations on biomolecules. I. The method. *J. Comput. Chem.* **1992**, *13*, 1011−1021.
(53) Janke, W. Monte Carlo simulations in statistical physics − From basic principles to advanced applications. In *Order, Disorder and Criticality: Advanced Problems of Phase Transition Theory*; Holovatch, Y., Ed.; World Scientific: Singapore, 2013; Vol. 3; pp 93−166.
(54) Efron, B. *The Jackknife, the Bootstrap and Other Resampling Plans*; Society for Industrial and Applied Mathematics: Philadelphia, 1982.
(55) Virnau, P. Detection and visualization of physical knots in macromolecules. *Phys. Procedia* **2010**, *6*, 117−125.
(56) Janke, W.; Marenz, M. Stable knots in the phase diagram of semiflexible polymers: A topological order parameter? *J. Phys.: Conf. Ser.* **2016**, *750*, 012006.
(57) Förster, S.; Widdra, W. Structure of single polythiophene molecules on Au(001) prepared by in situ UHV electrospray deposition. *J. Chem. Phys.* **2014**, *141*, 054713.
(58) Förster, S.; Kohl, E.; Ivanov, M.; Gross, J.; Widdra, W.; Janke, W. Polymer adsorption on reconstructed Au (001): A statistical description of P3HT by scanning tunneling microscopy and coarse-grained Monte Carlo simulations. *J. Chem. Phys.* **2014**, *141*, 164701.
(59) Kremer, K.; Grest, G. S. Dynamics of entangled linear polymer melts: A molecular-dynamics simulation. *J. Chem. Phys.* **1990**, *92*, 5057−5086.
(60) We thank D. Seaton and S. Schnabel for providing the parameters they used in ref 12.

https://doi.org/10.1021/acs.macromol.0c02584
Macromolecules 2021, 54, 5321−5334